Received: 21 May 2021 | Revised: 18 November 2021 | Accepted: 28 December 2021

DOI: 10.1002/aic.17635

AIChE JOURNAL

RESEARCH ARTICLE

Transport Phenomena and Fluid Mechanics

Thermal conductivity of the ionic liquid [HMIm][Tf_2N] with compressed carbon dioxide

Karim S. Al-Barghouti[1,2] | Aaron M. Scurto[1,2]

[1]Department of Chemical & Petroleum Engineering, University of Kansas, Lawrence, Kansas, USA

[2]Center for Environmentally Beneficial Catalysis, University of Kansas, Lawrence, Kansas, USA

Correspondence
Aaron M. Scurto, Department of Chemical & Petroleum Engineering, University of Kansas, Lawrence, KS 66045, USA.
Email: ascurto@ku.edu

Funding information
National Science Foundation, Grant/Award Numbers: CBET-1917480, EEC-1852308, EFRI-2029354

Abstract

The liquid thermal conductivity of the ionic liquid (IL), 1-hexyl-3-methyl-imidazolium bis(trifluoromethylsulfonyl)amide ([HMIm][Tf_2N]), saturated with compressed vapor and supercritical carbon dioxide was measured over three isotherms (298.15, 323.15, and 348.15 K) and pressures up to approximately 20 MPa using a transient hot-wire technique. Pure [HMIm][Tf_2N] thermal conductivity was also measured over a temperature range of 293.15–353.15 K at ambient pressure and with hydrostatic pressure to approximately 20 MPa. Literature vapor–liquid equilibrium data were used to predict the liquid CO_2 composition at the conditions investigated. Initially, the liquid thermal conductivity slightly decreased with pressure/composition of CO_2 followed by a gradual increase that is mainly attributed to hydrostatic pressure effects. Simple composition-based mixing rules for mixture properties are not qualitatively nor quantitatively accurate. These data could be used to engineer heat transfer equipment required for a variety of proposed IL applications in CO_2 capture, absorption refrigeration, biphasic CO_2/IL reaction platforms, etc.

KEYWORDS
carbon dioxide, ionic liquid, thermal conductivity

1 | INTRODUCTION

The unique chemical and physical properties of ionic liquids (ILs) allow for their potential use in a multitude of engineering applications. ILs as a class can be molecularly tuned through various cations, anions, and functional groups to possess properties needed to optimize an application, whether a physical or chemical process. This diversity also renders simple categorization difficult. However, ILs are generally stable to moderate temperatures and are liquid over a wide temperature range with high flash points (generally when they decompose).[1] Moreover, most ILs possess negligible volatility which is an advantage over conventional organic solvents where air pollution is a primary concern. Such exceptional properties of ILs allow for their potential use in a wide variety of applications such as interfacial films in catalytic reactions,[2,3] entrainers in extractive distillation,[4] high-voltage electrolytes in lithium-ion batteries and fuel cells,[5,6] stationary phases in gas chromatography,[7] solvents in gas separations,[8–16] heat-transfer fluids in heat pumps and absorption refrigeration systems, etc.[17,18]

The combination of ILs and compressed gases, especially carbon dioxide, is of particular interest in some of the leading applications. It has been shown by various groups that ILs can be tuned to have high solubility of carbon dioxide (>70% mole). ILs are actively being studied for CO_2 capture, whether in a pre- or postcombustion scenario,[19–28] where their lack of volatility would lead to little solvent loss. Precombustion CO_2 capture removes carbon dioxide from a gasified hydrocarbon source (e.g., coal) generally at high pressure. In contrast, postcombustion technology separates carbon dioxide from the exhaust gas from combustion, generally at lower or near-ambient pressure and low partial pressures of CO_2.[29] CO_2 removal from natural gas sources has also been studied.[26,30] Absorption refrigeration using CO_2 as a refrigerant and an IL as an absorbing liquid has been proposed.[31–34]

What is often overlooked in gas absorption in ILs is the required heat management. For example, the heat of vaporization of pure CO_2 at 298.15 K is approximately 120 kJ/kg.[35] While the thermodynamic heat of absorption of CO_2 into ILs will be different depending on the

IL solvent, it will generally be in the same order of magnitude for physical solubility. For adiabatic absorption, the temperature will increase upon CO_2 dissolution which will decrease the thermodynamic solubility, thus decreasing the capacity of the IL. Moreover, the CO_2 is generally recovered from ILs by heating, vacuuming, or gas stripping, any of which will require some addition of heat for near isothermal operation. Lower temperatures will result in higher residual CO_2 in the IL. Thus, heat transfer engineering will be important for the IL/CO_2 mixtures.

Another area of interest is in reactions and catalysis in biphasic systems of ILs and compressed CO_2. These are a subset of what have been termed gas-expanded liquids (GXLs) or specifically CO_2-expanded liquids (CXLs)[36] and experience only modest volume expansion upon dissolution of CO_2. In one scenario, the IL phase sequesters the catalyst, and the compressed (or supercritical) CO_2 phase can bring in reactants and remove products. A large variety of chemistries and catalysts have been investigated.[3,37-47] We have investigated using biphasic IL/CO_2 systems for the hydrogenation and hydroformylation of olefins using homogeneous catalysts and have observed the interplay of phase equilibrium thermodynamics, and mass transfer to help engineer these systems.[3,48] Most of these studies concern exothermic reactions, and proper cooling would be needed for scale-up processes to prevent safety issues and poor product quality. Thus, thermal properties of the IL mixture are needed.

To properly design and scale-up any of these applications involving ILs and carbon dioxide, thermodynamic data as well as transport data (heat, mass, and momentum) are needed. Numerous groups (including our own) have studied the solubility (phase equilibrium) of a wide variety of gases, especially CO_2, in ILs.[15,49-64] However, there are significantly fewer studies on the transport properties (viscosity, diffusivity, and thermal conductivity) of ILs especially in mixtures with compressed gases. We have measured the viscosity of ILs (imidazolium and pyrrolidinium ILs) saturated with compressed CO_2.[65,66] Various groups have measured the Fickian diffusion coefficient of CO_2 into several types of ILs.[64,67-74]

Limited studies on thermal properties of pure ILs have been conducted by various groups for pure ILs and even less for IL mixtures. Frez et al.[75] reported the thermal conductivities of four imidazolium-based pure ILs at room temperature using a thermal grating technique with literature values for the densities and specific heats. Fröba et al.[76] measured the thermal conductivity of a series of pure ILs over the temperature range of 273.15–333.15 K using a guarded parallel-plate method that utilizes a single-dimensional form of Fourier's Law of heat conduction. Ge et al.[77] utilized a transient hot-wire method to measure the thermal conductivity of 11 different ILs over a temperature range of 293–353 K. Further simulations and experiments on thermal and transport properties of pure ILs have been conducted by various groups.[78-89] Gardas and Coutinho[90] have utilized a group contribution model to predict the thermal conductivity of certain ILs as a function of temperature and two contribution fitting parameters. Wu et al.[91] have also developed a group contribution method to predict the thermal conductivity of ILs at atmospheric pressure. Chen et al.[92] investigated the effects of ethanol and water on the thermal conductivity of 1-ethyl-3-methylimidazolium ethylsulfate ([EMIm][$EtSO_4$]) over the temperature range of 283.15–343.15 K. Yebra et al.[80] and Tomida et al.[93] reported on the pressure effects on thermal conductivity of various ILs.

While the heat transfer properties of pure ILs are important, thermal properties of mixtures with ILs will be vitally important for design and scale-up. Thermal conductivity of such mixtures would be needed to design, for instance, heat exchangers in absorption or extractive distillation columns; size heat generators in absorption-refrigeration cycles; and optimally design heat pumps among other applications. However, the availability in the literature of thermal conductivity data of any liquid saturated with any gas is scarce and for ILs, only a couple of studies exist. We have recently reported the thermal conductivities of CO_2 saturated *n*-alkanes.[94] Tomida et al.[95] conducted one of the first studies on the thermal conductivity of sub-saturated mixtures of CO_2 with the ILs 1-butyl-3-methylimidazolium hexafluorophosphate ([BMIm][PF_6]) and 1-butyl-3-methylimidazolium tetrafluoroborate ([BMIm][BF_4]) over a temperature range of 294–334 K and mole fractions of CO_2 up to 0.42. Rausch et al.[96] measured the thermal diffusivity (related to the thermal conductivity by the density and heat capacity) of CO_2-saturated 1-butyl-3-methylimidazolium tricyanomethanide ([BMIm][$C(CN)_3$]) and 1-butyl-3-methylimidazolium tetracyanoborate ([BMIm][$B(CN)_4$]) ILs over the temperature range of 303.15–333.15 K and CO_2 compositions up to 0.393 using a dynamic light scattering technique. Klein et al.[97] determined the thermal and mutual diffusivities of [AMIm][Tf_2N] ILs with several dissolved gases (including CO_2) near infinite dilution utilizing dynamic light scattering techniques and molecular dynamics simulations.

Herein, a transient hot-wire method was utilized to measure and report the thermal conductivity of a biphasic IL/CO_2 system over three isotherms (298.15, 323.15, 348.15 K) with varying molar compositions of the introduced CO_2. The thermal conductivity of pure 1-hexyl-3-methylimidazolium bis(trifluoromethylsulfonyl)amide ([HMIm][Tf_2N]) over the temperature range 298.15–353.15 K is also reported and compared to literature data. Thermal conductivity values for ([HMIm][Tf_2N]) saturated with CO_2 (Table 1) have been measured and reported in this study.

2 | EXPERIMENTAL METHODS

2.1 | Thermal conductivity

A transient hot-wire method was employed to measure thermal conductivity. Detailed analysis of the transient hot-wire method has been carried out by various investigative groups and the methodology has been reported in the literature.[94,98,99] We have previously reported on the use of this apparatus to measure the thermal conductivity of various systems such as CO_2-expanded hydrocarbons.[94,100,101] An overview of the methodology will be given here. A transient-hot wire sensor manufactured by Flucon Fluid Control GmbH (Lambda instrument) has been coupled with a custom-built in-house high-pressure vessel with a view cell and an attachable heating/cooling jacket. A short-term current is applied to the wire to induce Joule heating while the RTD follows the localized temperature. The cylinder as well as the fluid surrounding the wire are assumed to be isotropic and infinite in

TABLE 1 Specifications of chemicals used in this study

Full name	Chemical structure	CAS	Source	Purity
1-Hexyl-3-methyl-imidazolium bis(trifluoromethylsulfonyl) amide	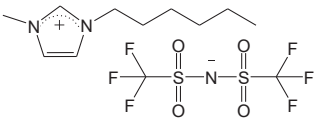	382150-50-7	IoLiTec	99+%[a]
Carbon dioxide	O═C═O	124-38-9	MATHESON	99.995%[b]

Abbreviations: CAS, Chemical Abstract Services; NMR, Chemical Abstract Services.
[a]Reported by manufacturer and confirmed here by NMR analysis.
[b]Specified by supplier.

all spatial dimensions. A single-dimension heat conduction leads to a simplified Fourier correlation:

$$\frac{\partial T}{\partial t} = \frac{\lambda}{C_p \cdot \rho}\left(\frac{\partial^2 T}{\partial r^2} + \frac{1}{r}\frac{\partial T}{\partial t}\right) \quad (1)$$

In which T is the temperature of the wire, r is the radius of the wire, λ is the thermal conductivity of the fluid, C_p is the specific heat capacity of the fluid, ρ is the density of the fluid, and t is time.

The solution to Equation (1) has been reported by Carslaw and Jaeger[102] as the following:

$$T_t - T_0 = -\frac{Q}{4\pi\lambda} E_i\left(-\frac{r^2 C_p \cdot \rho}{4\lambda t}\right), \quad (2)$$

where Q is the input heat per unit length and E_i is the exponential integral defined as follows:

$$E(x) = \int_{-\infty}^{x} \frac{e^t}{t} dt \quad (3)$$

When t (time following the induction of heat through the wire) is orders of magnitude greater than $\frac{r^2 C_p \cdot \rho}{4\lambda}$, the first term of the exponential integral provides an accurate approximation as follows:

$$T_t - T_0 = \frac{Q}{4\pi\lambda}\left(\ln\left(\frac{4t}{r^2 C_p \cdot \rho}\right) - \gamma\right) \quad (4)$$

γ = Euler–Mascheroni constant (~0.577).

Consequently, the Flucon LAMBDA system calculates the thermal conductivity as a function of two heat input points at two different times with respect to the temperature difference between the two time points:

$$\lambda = \frac{Q_{t_1} - Q_{t_2}}{8\pi(T_{t_2} - T_{t_1})} \ln\frac{t_2}{t_1} \quad (5)$$

Important constraints governing the feasibility and accuracy of the measurements include a minimum fluid sample to cover the wire, low convection (either forced or natural), relatively isotropic fluid and boundaries, and ample time allowed after induction of heat through the wire. An investigation on the minimum fluid sample needed for the infinite medium assumption to be applicable has been carried out by Cohen and Glicksman.[99] Applying the correlation for the related upper limit of the fluid sample to the systems investigated herein illustrates that the fluid volume used is some orders (>10x) greater than the upper limit of the minimum fluid sample required. For Equation (4) to be applicable with minimal error introduced, the time required must be greater than 5 ms. The LAMBDA device is automatically programmed to introduce measurements of no smaller time intervals. In addition, the device may be manually programmed to change the default time interval between the measurements.

The platinum wire has a diameter of 0.1 mm and a length of 35 mm. The sensor head is equipped with a Pt100 resistance temperature detector that reports the temperature of the fluid with an accuracy of ±0.1 K. The vessel has a smaller diameter for the bottom portion of the cell for the liquid phase and a larger diameter in the upper portion of the cell for the vapor phase to allow for volume expansion of the liquid throughout the pressure range. Approximately 38 mL of liquid is required to completely cover the wire. The total volume of the vessel is 143.42 mL and allows for approximately 300% volume expansion of the liquid phase before the biphasic vapor–liquid equilibrium scenario can no longer be confirmed. The window also allows for confirmation that the wire is covered by the liquid phase. The liquid was stirred with a magnetic stir bar and stir plate. A high-pressure syringe pump, Teledyne-Isco, Inc. 100DM, was used to generate the gas pressure. The vessel sits in a modified heating/cooling jacket that is connected to a Fisher Scientific Isotemp 3016 heated bath circulator with a temperature stability of ±0.01 K. An OMEGA DPG7000-3K pressure gauge capable of 3000 psi (20.68 MPa) with a 0.05% full-scale accuracy (±0.01 MPa) was mounted on the vessel.

As the theory of the transient hot-wire technique has several assumptions, for example, an infinite cylinder, and so forth, a one-point calibration method with a standard fluid is used to account for end-effects, and so forth. *n*-Heptane was used as its thermal conductivity values[35,103,104] are of the same order as those for the pure [HMIm][Tf_2N]. Once the device is calibrated, the IL is loaded into the smaller cylindrical portion of the vessel. The platinum wire and the temperature detector portion of the sensor are then immersed in the IL. The heating bath is set to the temperature of interest and thus, circulates a mixture of heated propylene glycol and deionized water in the vessel's heating/cooling jacket. Once the temperature of interest is attained, the heating bath is turned off and allowed to rest for some time before measurements are taken (on the order of a few minutes).

Allowing the circulating water to rest before taking measurements is essential to reducing any induced convections due to vibrations.

For the measurements involving biphasic systems of IL/compressed gas, the IL is introduced to the vessel and sealed. A vacuum (~7 kPa) is used for ~24 h to remove any gas and moisture introduced in the transfer process. The gas of interest is introduced using the high-pressure syringe pump. A magnetic stir bar and stir plate are used to attain vapor–liquid equilibrium. Once equilibrated, the stirring and circulation in the heating/cooling jacket are turned off and adequate time is allowed to produce a quiescent liquid phase for the measurements. A simple study of pressure decay and thermal conductivity stability with stirring time shows that approximately 40 min is required to reach equilibria and stability. In the measurements conducted, stirring was carried out for 60 min using a Polytetrafluoroethylene, PTFE-coated magnetic stir bar (D = 2 mm; L = 6 mm). Equilibria data reported in the literature are used to correlate the pressure of the system to the composition of the introduced gas.

The thermal conductivity with hydrostatic pressure was investigated in a similar system as described above. The IL was injected into the pressure vessel and allowed to overflow into about ~3+ cm of the 1/16^{00} tubing with 0.030-inch inner diameter leading to the syringe pump. Helium was loaded into the syringe pump to provide the hydrostatic pressure rather than filling the pump with the IL itself. Helium solubility data are not available in [HMIm][Tf_2N] beyond infinite dilution regimes. However, data on the estimated solubility and diffusivity data of helium in 1-ally-3-methylimidazolium [AMIm][Tf_2N] were reported by Klein et al.[97] with estimated compositions of He in the IL. They estimated a small but finite solubility of helium in this IL over the pressure range. Based on the small solubility and the diffusivity, the rate at which helium diffused down the tubing and into the thermal conductivity cell was estimated to be negligible over the time frame of the measurements (calculated at <0.005 mole fraction after 2 h).

2.2 | Uncertainty

The nominal uncertainty associated with the thermal conductivity sensor given by the manufacturer is ±1%. However, we have measured the thermal conductivity of *n*-alkanes in a previous study[94] and found much less error; *n*-alkanes (e.g., C6–C14) have thermal conductivities that overlap those of the IL in this study. For instance, the difference between our measurements for *n*-hexane and *n*-tetradecane at three temperatures and well-established experimental values had an average absolute relative deviation (AARD) of 0.25%. Thus, we believe the inherent error in the measurement to be approximately ±0.3 mW/m K. We obtain measurement-to-measurement precision for these IL systems of approximately ±0.03 mW/m K at the lower temperatures (298.15 and 323.15 K) which climbs to ±0.3 at 348.15 K. The run-to-run (day-to-day) repeatability is approximately ±0.1 mW/m K The main source of uncertainty associated with the reproducibility of the data is any type of convection due to vibrations, natural convection from the heat jacket, and so forth. We estimate that the total uncertainty to be approximately ±0.3 mW/m K at 298.15 K and 323.15 K rising to ±0.6 mW/m K at 348.15 K. The Pt100 temperature probe has an uncertainty of ±0.1 K. The pressure gauge utilized has a reported uncertainty of ±0.01 MPa. Thermal control of the system is ±0.1 K. Another potential source of error is associated with interpolation of literature vapor–liquid equilibria (VLE) data to predict the composition of the gas in the IL at the given temperature and pressure of the thermal conductivity measurements. To assess the uncertainty accompanying the interpolated values, the equilibria data at each pressure value was fit to a second-order polynomial and the maximum possible deviation at each value was calculated. The average deviation among the fit data is approximately 2.5% with a maximum deviation of 8% occurring in the lower pressure region (lowest compositions).

2.3 | Chemicals

The IL 1-hexyl-3-methyl-imidazolium bis(trifluoromethylsulfonyl) amide (CAS#382150-50-7) was purchased from IoLiTec. The specified purity is 99% (Table 1). The IL was further dried under vacuum and a Mettler Toledo C20S Karl Fisher (KF) Coulometer was used to determine the water content. The water content of the pure IL before and after the measurements were completed was measured and determined to be less than 125 ppm in all cases (average of three KF trials each with a mass content between 1.5 and 3 g of sample). Proton Nuclear Magnetic Resonance spectrometer (NMR) analysis was performed to determine the purity of the IL sample and the purity was estimated to be 99% + % as no peaks associated with contaminants were detected. Ultra-high purity (99.995%) carbon dioxide purchased from MATHESON was used.

3 | RESULTS AND DISCUSSION

3.1 | Pure [HMIm][Tf_2N] thermal conductivity

The transient hot-wire method employed in this study was first confirmed on pure 1-hexyl-3-methyl-imidazolium bis(trifluoromethylsulfonyl) amide ([HMIm][Tf_2N]) thermal conductivity. Table 2 and Figure 1 illustrate the dependence of thermal conductivity on temperature. The thermal conductivity of the pure IL decreases with increasing temperature at constant pressure. The values obtained in this study, as well as literature values[76,77,91,105,106] over the temperature range, are shown in Figure 1. The thermal conductivity of the pure IL decreases with increasing temperature for our data. For values measured in this study, the percent decrease in thermal conductivity from 293.15 to 353.15 K is 4.3%. Except for the data reported by Paredes et al.,[105] the general trends in thermal conductivity as a function of temperature are similar among the reported literature values in which the thermal conductivity decreases with increasing temperatures. The largest deviations in values among the various literature data sets as well as the data measured in this study are observed at the higher temperatures. The standard deviation among all the data sets included in Figure 1 at 353.15 K is 2.93 with a 95%

TABLE 2 Experimental thermal conductivity of [HMIm][Tf_2N]

T (K)	λ (mW/m-K)
293.15	128.91
298.15	128.43
303.15	128.00
313.15	126.36
323.15	124.98
333.15	124.11
343.15	123.80
348.15	123.75
353.15	123.40

Note: Standard uncertainties: $u(T)$ = 0.1 K; $u(\lambda)$ = 0.3 mW/m-K from 298.15 to 323.15 K and $u(\lambda)$ = 0.6 mW/m-K at higher temperatures.
Abbreviation: [HMIm][Tf_2N], 1-hexyl-3-methyl-imidazolium bis(trifluoromethylsulfonyl)amide.

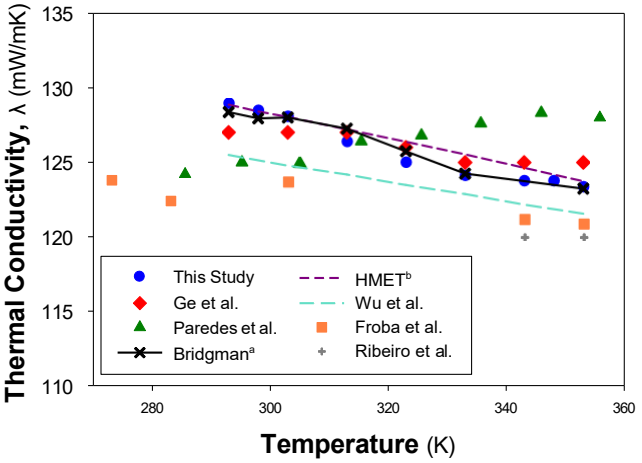

FIGURE 1 Thermal conductivity of pure [HMIm][Tf_2N] with temperature; ( ) this study; ( ) Ge et al.[77]; ( ) Fröba et al.[76]; ( ) Paredes et al.[105]; (+) Ribeiro et al.[106]; [a]Smoothed Bridgman Correlation (Equation 6) and [b]HMET Correlation (Equation 7); (dashed cyan line) Wu et al.[91]-group contribution prediction. [HMIm][Tf_2N], 1-hexyl-3-methyl-imidazolium bis(trifluoromethylsulfonyl)amide; HMET, Heuristic Modification of the Enskog Theory

confidence interval of 123.48± 2.57 mW/m K. The %AARD between data presented in this study for the thermal conductivity of pure [HMIm][Tf_2N] and the data reported by Ge et al.[77] is less than 1% for the temperature range of 293–353 K. The data presented in this study are also in good agreement with that reported by Fröba et al.[76] The data reported by Tenney et al.[79] and Frez et al.[75] were omitted from the graph since they report a single averaged value over a temperature range. The percent difference between the thermal conductivity obtained in this study at 323.15 K and that of Fröba et al.[75] at the same temperature is approximately 2.5%. Fröba et al.[75] utilized a guarded parallel-plate method in contrast to the transient hot-wire method employed in this study. Tenney et al.[79]

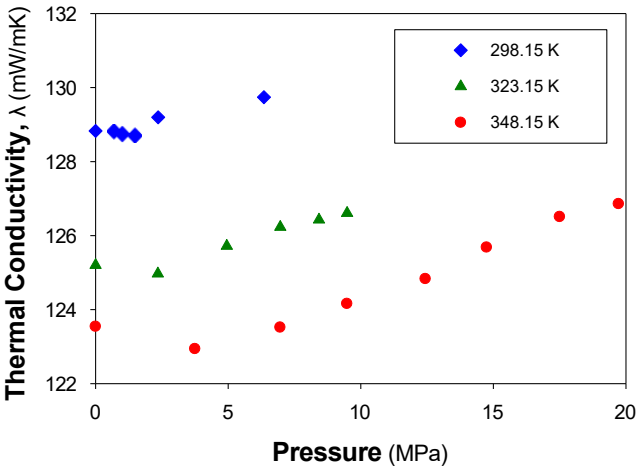

FIGURE 2 Thermal conductivity of [HMIm][Tf_2N]/CO_2 at saturation at various pressures and three isotherms; (◆) 298.15 K; (▲) 323.15 K; (●) 348.15 K. [HMIm][Tf_2N], 1-hexyl-3-methyl-imidazolium bis(trifluoromethylsulfonyl)amide

used a guarded heat flow meter method while Frez et al.[75] used a transient grating technique.

A modified Bridgman correlation[107] has been reported in the literature to correlate the thermal conductivity of ILs:

$$\lambda = k\rho^{\delta 2=3}MW^{\delta 1=3}cC_v, \quad (6)$$

where ρ is the mass density, MW is the molecular weight, c is the speed of sound, C_v is the isochoric heat capacity, and k is a constant parameter regressed to the data by minimizing the %AARD relative to the experimental values. We attempted to use this correlation to confirm the qualitative trends observed for the thermal conductivity of [HMIm][Tf_2N]. Values for density were obtained from data reported by Esperança et al.[108] and Safarov et al.[109] Data for the speed of sound were obtained from data reported by Andresová et al.[110] The isochoric heat capacity values used were interpolated from the data of Polikhronidi et al.[111] The reported isochoric heat capacity data show a quadratic dependence on temperature with a general increase in isochoric heat capacity with temperature. Figure 1 illustrates the Bridgman equation correlated to our data (k = 8.234 x 10^{-10}) and fits the data very well including the prediction of a negative slope for the thermal conductivities with temperature.

A Heuristic Modification of the Enskog Theory (HMET) as described by Yebra et al.[80] has also been utilized to correlate the trends in pure IL thermal conductivity (Figure 2). The variation of the HMET correlation utilized for the purpose of this study is shown in Equation (7).

$$\lambda = A + B\,ln(\rho) + 0.5\ln(T), \quad (7)$$

where A and B are parameters fit to the data, ρ is the density in kg/m^3 (from Esperança et al.[108] and Safarov et al.[109]), and T is temperature

TABLE 3 Thermal conductivity, CO_2 composition, fractional volume expansion, and molar volume of CO_2 saturated [HMIm][Tf_2N]

T (K)	P (MPa)	x_{CO_2}	λ (mW/m-K)	λ/λ_0	$\Delta V/V_0$	V^E (cm³/mol)
298.15[a]	0[b]	0.00	128.83	1.000		
	0.71	0.14	128.82	1.000	0.02	285
	1.01	0.20	128.75	0.999	0.03	268
	1.47	0.29	128.71	0.999	0.05	245
	2.36	0.44	129.2	1.003	0.21	206
	6.35	0.75	129.74	1.007	0.37	114
323.15[a]	0[b]	0.00	125.20	1.000		
	2.35	0.32	124.97	0.998	0.08	240
	4.95	0.56	125.72	1.004	0.15	179
	6.96	0.65	126.23	1.008	0.24	152
	8.42	0.71	126.43	1.010	0.30	135
	9.48	0.74	126.61	1.011	0.33	124
348.15[a]	0[b]	0.00	123.54	1.000		
	3.75	0.26	122.94	0.995	0.07	271
	6.96	0.47	123.52	1.000	0.14	210
	9.48	0.58	124.16	1.005	0.20	174
	12.44	0.67	124.83	1.010	0.27	147
	14.75	0.71	125.68	1.017	0.30	133
	17.50	0.74	126.51	1.024	0.33	128
	19.72	0.76	126.86	1.027	0.34	123

Note: Reported standard uncertainties: $u(T)$ = 0.1 K; $u(P)$ = 0.01 MPa; $u(\lambda)$ = 0.3 mW/m-K at 298.15 and 323.15 K and $u(\lambda)$ = 0.6 mW/m-K at 348.15 K; $u(V^E)$ = 1 cm³/mol; $u(x)$ = 0.02; $u(\Delta V/V_0)$ = 0.01.
Abbreviation: [HMIm][Tf_2N], 1-hexyl-3-methyl-imidazolium bis(trifluoromethylsulfonyl)amide.
[a]Compositions, volume expansions, and molar volumes were interpolated/extrapolated from the data of Ren and Scurto.
[b]Pure IL at ambient pressure (gauge).

in absolute Kelvin. The constant parameters, A and B, were fit to the data by minimizing the %AARD relative to the experimental data, where A = -795.51 and B = 127.50. With its two-regressed parameters, the HMET equation was expected to well correlate the data.

Based on the data pertinent to this study, the pure IL thermal conductivity can be empirically correlated over the temperature range 293.15–353.15 K using a second order polynomial as follows:

$$\lambda \text{¼} 1{:}256 \times 10^{-3}\eth T\text{Þ}^2 - 9{:}086 \times 10^{-1}\eth T\text{Þ} \text{þ} 287{:}6 \qquad \eth 8\text{Þ}$$

In which T is the temperature of the pure IL in absolute Kelvin and within the range 293.15 K < T < 353.15 K. The average uncertainty, $u(\lambda)$, associated with predicted values obtained using Equation (8) is $u(\lambda)$ = 0.2 mW/m K.

3.2 | CO_2 saturated [HMIm][Tf_2N] thermal conductivity

The thermal conductivity of [HMIm][Tf_2N] saturated with CO_2 has been measured over three isotherms (298.15, 323.15, 348.15 K) and pressures up to 19.7 MPa. On average, the thermal conductivity remains relatively constant with the pure IL thermal conductivity along the entirety of the pressure range in which the greatest change in thermal conductivity relative to the pure IL thermal conductivity is approximately 2.7%. However, despite the relatively small net change, the behavior of the [HMIm][Tf_2N]/CO_2 system demonstrates distinct and changing trends with temperature and pressure. For all isotherms, there is a slight decrease in thermal conductivity at lower pressures followed by a relatively larger increase in thermal conductivity at higher pressures. The change in thermal conductivity at 298.15 K with pressure shows a gradual, slight decrease with pressures up to approximately 1.5 MPa followed by a gradual increase along the rest of the pressure range investigated. The maximum pressure investigated at 298.15 K is just below the pressure at which vapor–liquid–liquid equilibrium (VLLE) occurs for this system as reported by Ren et al.[63] The thermal conductivity at a pressure of 6.35 MPa has a value approximately 0.7% greater than the pure IL thermal conductivity at 298.15 K. Similar trends are observed at 323.15 and 348.15 K in which the thermal conductivity decreases slightly at lower pressures then increases gradually with increased pressure. The values at the minima are beyond the experimental uncertainty.

VLE data of this system from Ren et al.[63] were interpolated for the same temperature and pressure range of the thermal conductivity measurements (Table 3) to understand the phenomena in terms of temperature, pressure, and composition. We believe that the

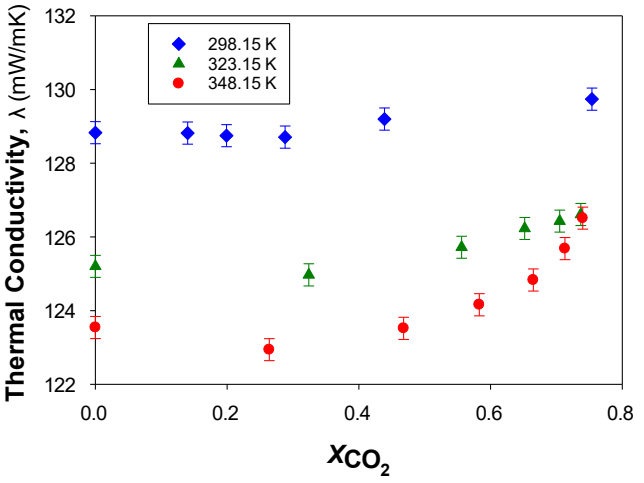

FIGURE 3 Thermal conductivity of [HMIm][Tf_2N]/CO_2 at saturation at various compositions and three isotherms; (◆) 298.15 K; (▲) 323.15 K; (●) 348.15 K. [HMIm][Tf_2N], 1-hexyl-3-methyl-imidazolium bis(trifluoromethylsulfonyl)amide

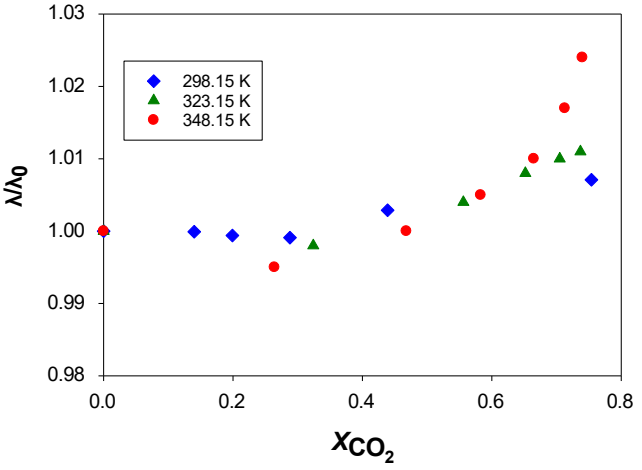

FIGURE 4 Normalized thermal conductivity (λ/λ_0) of [HMIm][Tf_2N]/CO_2 at various compositions and three isotherms; (◆) 298.15 K; (▲) 323.15 K; (●) 348.15 K. [HMIm][Tf_2N], 1-hexyl-3-methyl-imidazolium bis(trifluoromethylsulfonyl)amide

interpolations are accurate to approximately 2%–3%. CO_2 has a relatively high solubility in the IL over the pressure range. For instance, the solubility at 348.15 K and 14.7 MPa is approximately 71% mole. Thermal conductivity in relation to the composition of the gas is illustrated in Table 3 and Figure 3. The thermal conductivity of the mixture remains in relative proximity to that of the pure IL despite large solubility of CO_2 in the system. At a 76%mole CO_2 in the mixture, the thermal conductivity changes by approximately 2.7% relative to the pure IL thermal conductivity.

Figure 3 illustrates that the thermal conductivity of the CO_2-expanded IL shows only a slight dependence on the composition of CO_2 in the mixture. The minimum occurs below 40% mole CO_2 at each isotherm followed by increasing thermal conductivity at higher compositions. These higher compositions correspond to higher system pressures. At 323.15 K and a CO_2 molar composition of 32%mole, the thermal conductivity decreases by approximately 0.2% relative to the pure IL thermal conductivity at the same temperature. At the same temperature and a CO_2 molar composition 74%mole, the thermal conductivity increases by approximately 1.1% relative to the pure IL thermal conductivity. A similar trend is observed at 348.15 K in which the thermal conductivity decreases slightly at low to moderate CO_2 compositions to then increase as the composition of CO_2 increases.

The ratios of the thermal conductivity at different compositions and temperatures relative to the thermal conductivity of the pure IL at the same temperature and ambient pressure is illustrated in Figure 4. Below approximately 70% mole CO_2, the relative thermal conductivities are similar at the same composition. The thermal conductivity of the mixture slightly decreases with initial compositions of CO_2 to a similar extent at all the temperatures investigated. This is followed by a similar increase starting around 40%mole at all temperatures. However, at compositions above approximately 70% mole, both absolute and relative changes are different among the three temperatures, with the relative increase in thermal conductivity increasing with temperature. The reason for the change in correlation with temperature at the highest compositions is likely due to the vastly different pressures (see below) needed to create similar solubilities. For instance, the pressure needed to obtain approximately 75% mole CO_2 at 298.15 K is ~6.4 MPa vs. 9.5 MPa at 323.15 K vs. 19.7 MPa at 348.15 K.

Figure 5 illustrates the thermal conductivity at 298.15 K with CO_2 composition in addition to the pure saturated liquid CO_2 thermal conductivity at the same temperature (and at its vapor pressure of 6.34 MPa) from literature[35,112] and the pure IL thermal conductivity at ambient pressure measured here. The line in the figure represents a simple linear mixing rule of the pure component properties with composition which correlates with the initial decrease in the thermal conductivity with increasing composition. As pure CO_2 has a much lower thermal conductivity, one might expect the mixture conductivity of the IL phase to decrease due to composition effects: diluting a relatively high thermal conductivity component with a lower thermal conductivity component. However, there is no smooth and linear method to connect the falling and rising mixture data with pure component properties and the compositions. Such a linear approximation would significantly underpredict the mixture properties throughout the entire composition range. This is of practical importance for the design and scale-up of compressed gas (CO_2) systems with ILs discussed in the introduction. This underprediction would result in the design of much larger equipment (higher surface area) than needed, for example, heat exchangers, reboilers, and so forth, which would result in a higher cost.

A mixing rule or correlation for this CO_2 and IL system is also complicated by the phase behavior. From our previous study and other literature sources, ILs and CO_2 form a Type III system by the classification of Scott and van Konynenburg.[113] Type III systems are characterized by either liquid–liquid, vapor–liquid, or vapor–liquid–liquid equilibria which do not terminate at mixture critical points

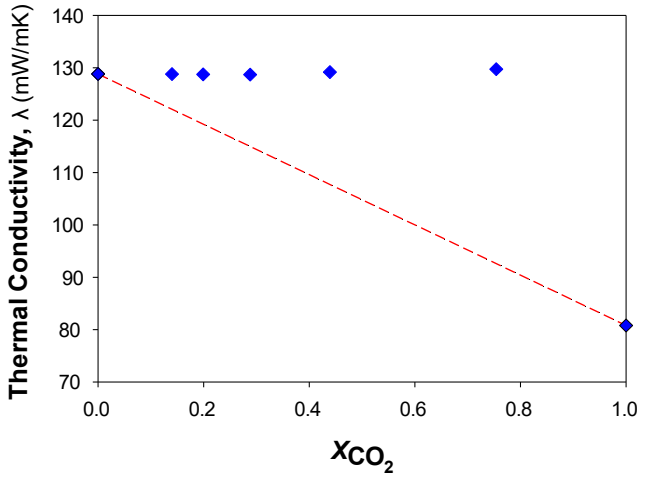

FIGURE 5 Thermal conductivity of [HMIm][Tf_2N]/CO_2 at 298.15 K with composition using the pure saturated liquid thermal conductivity from NIST REFPROP.[35] The line is a linear mixing rule using composition. [HMIm][Tf_2N], 1-hexyl-3-methyl-imidazolium bis(trifluoromethylsulfonyl)amide

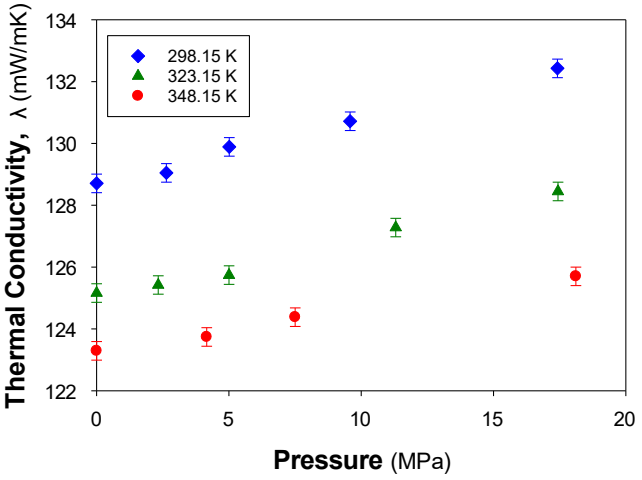

FIGURE 6 Thermal conductivity of pure [HMIm][Tf_2N] with pressure and temperature; (◆) 298.15 K; (▲) 323.15 K; (●) 348.15 K; *u* (λ) = 0.3 mW/m-K. [HMIm][Tf_2N], 1-hexyl-3-methyl-imidazolium bis(trifluoromethylsulfonyl)amide

(L = L or V = L) except, theoretically, at ultra-high pressures (which have never been experimentally seen with IL/CO_2 systems even to kilobar pressures). The isotherm at 298.15 K for this [HMIm][Tf_2N]/CO_2 system is below the upper critical endpoint (UCEP, ~304 K), thus higher pressure will result in VLLE followed by LLE, but never a single miscible IL phase. The isotherms above 304 K will thus be VLE and only theoretically become critical as pressure tends to infinity. This implies that the conditions for our thermal conductivity measurements will never permit a single liquid phase from 100% IL to 100% CO_2 at any temperature.

It is hypothesized that the observed behavior of the liquid thermal conductivity of the IL and CO_2 is the consequence of two competing phenomena: (1) composition effects and (2) hydrostatic pressure effects. At lower pressures/compositions, the CO_2 contributes slightly to a decrease in thermal conductivity due to dilution with a lower thermal conductivity fluid, CO_2. If composition were the only effect, then only a decrease in thermal conductivity of the liquid mixture would be expected with increasing CO_2 composition. However, there is a minimum followed by an increase in thermal conductivity.

The behavior for CO_2 in ILs is quite different than other more polar gases. For instance, we are currently measuring the thermal conductivity of [1-alkyl-3-methyimidazolium][Tf_2N] ([RMIm][Tf_2N]) ILs saturated with compressed hydrofluorocarbon refrigerant gases, such as 1,1,1,2-tetrafluoroethane (R-134a).[114] As a Type V system, R-134a becomes miscible with [RMIm][Tf_2N] ILs at 298.15 K at its pure component vapor pressure of 0.67 MPa as 298.15 K is below the lower critical endpoint (LCEP). For this isotherm, thermal conductivity can be measured through the entire composition range. Here, the liquid thermal conductivity of the IL phase decreases rather linearly with moderate to large R-134a compositions (R-134a has a much lower thermal conductivity than the IL, like CO_2). However, even for this system, there is no simple correlation between composition and pure component thermal conductivity across the entire composition spectrum.

3.3 | Hydrostatic pressure effects on pure [HMIm][Tf_2N] thermal conductivity

The effect of hydrostatic pressure on the thermal conductivity of the pure IL was investigated to approximately 18 MPa to encompass the pressure range of the mixture results above. As illustrated in Figure 6, the thermal conductivity increases relatively linearly with increasing pressure. The thermal conductivity increases by ~2% at 298.15 K between ambient pressure and ~18 MPa. The increase of thermal conductivity as a function of pressure can also be attributed primarily to the increase in density at constant temperature, but also related to the speed of sound as predicted by the Bridgman correlation (Equation 6). The trends presented herein are similar to those reported by Yebra et al.[80] for several other ILs under pressure. From their data for the IL 1-butyl-3-methylimidazolium methylsulfate ([BMIm][$MeSO_4$]) at 293.15 K and 20 MPa, they report an increase of ~3%. Tomida et al.[93] also measured the thermal conductivity of several ILs under pressure. For the IL 1-hexyl-3-methylimidazolium hexafluorophosphate ([HMIm][PF_6]), Tomida et al.[93] report a thermal conductivity increase of ~2% from ambient pressure to 20 MPa at 294.1 K. Thus, the hydrostatic pressure effects for the IL/CO_2 system would be important in the pressure range investigated as the changes in the pure component over the pressure range, while relatively small, are of the same order of magnitude as the changes in the mixture properties. Rausch et al.[96] measured the thermal diffusivity of CO_2-saturated [BMIm][$C(CN)_3$] and [BMIm][$B(CN)_4$] ILs using a dynamic light scattering technique. Thermal diffusivity, α, is related to the thermal conductivity by:

$$\alpha = \frac{\lambda}{\rho C_p},$$

where ρ is the density and C_p is the isobaric heat capacity. Unfortunately, the density and heat capacity for these systems are not available to directly calculate and compare the thermal conductivity.

3.4 | Analysis of phenomenon

The data presented in this study illustrate that the thermal conductivity of the IL/CO_2 system is composed of two competing effects: (1) composition effects with the dissolution of CO_2 which has a significantly lower thermal conductivity; and (2) hydrostatic effects. It was noted above that simple mixing laws using the pure component thermal conductivities are not suitable in predicting the mixture thermal conductivity. As shown above, hydrostatic pressure effects may become important. Therefore, a composition mixing rule of the pure IL and CO_2 thermal conductivities adjusted for hydrostatic pressure effects was investigated:

$$\lambda_m = x_{IL}\lambda_{IL}(T,P) + x_{CO_2}\lambda^L_{CO_2}(T,P), \quad (9)$$

where, λ_m is the mixture thermal conductivity, x_i is the mole fraction of component i, and $\lambda_i(T,P)$ is the thermal conductivity of pure component i at the temperature and pressure of the mixture data. The pure component data for the IL at the temperature and pressure of interest, $\lambda_{IL}(T,P)$, is obtained by an interpolation of the data presented above. The pure liquid thermal conductivity of CO_2, $\lambda^L_{CO_2}(T,P)$, is extrapolated from the saturated liquid at T (and P^{sat} at T) as a function of pressure at the same temperature.[35,112] The change in thermal conductivity with pressure of pure liquid CO_2 is linear from its vapor pressure of 6.43 MPa (saturated liquid) to 10 MPa. Thus, this linear trend was then used to extrapolate down to the mixture pressure of interest. Figure 7 illustrates the pure IL and CO_2 thermal conductivities with pressure and the mixture results. As shown, even adjusting for hydrostatic pressure, the new mixing rule well underpredicts the data which are more closely correlated with that of the pure IL.

While thermal conductivity is not an equilibrium thermodynamic property, one could use the concept of an "excess" property to define the difference from an idealized solution, with "excess" thermal conductivity defined as follows:

$$\lambda^{EX}_m(T,P,x) = \lambda_m(T,P,x) - \left[x_{IL}\lambda_{IL}(T,P) + x_{CO_2}\lambda^L_{CO_2}(T,P)\right] \quad (10)$$

Figure 7 demonstrates that at the higher pressures and CO_2 compositions, this "excess" thermal conductivity becomes greater and greater with pressure and composition. For the isotherms greater than 304 K (CO_2 critical point), the extrapolations necessary for pure CO_2 increase in uncertainty (both theoretical, e.g., liquid properties of a supercritical fluid, and in practice) and are not performed.

Overall, the thermal conductivity behavior of the IL with initial amounts of CO_2 slightly decreases due to the composition of a lower thermal conductivity diluent. However, due to the phase behavior, the higher pressures required to increase the composition of the CO_2 commensurately increases the thermal conductivity due to hydrostatic effects. Various groups have asserted that CO_2 gas solubility in common ILs is dominated by the free volume available for the gas to occupy.[53,115–120] Thus, from the data, it can be reasoned that the introduced CO_2 does not alter the structure of the IL, nor solvate the IL or the individual cations and anions. Therefore, the IL retains the same mechanisms to conduct thermal energy whether as a pure IL or in the mixture. The slight increase in thermal conductivity at higher compositions of CO_2 is, in actuality, a pressure effect on the main underlying heat transfer mechanism which is dominated by the IL itself.

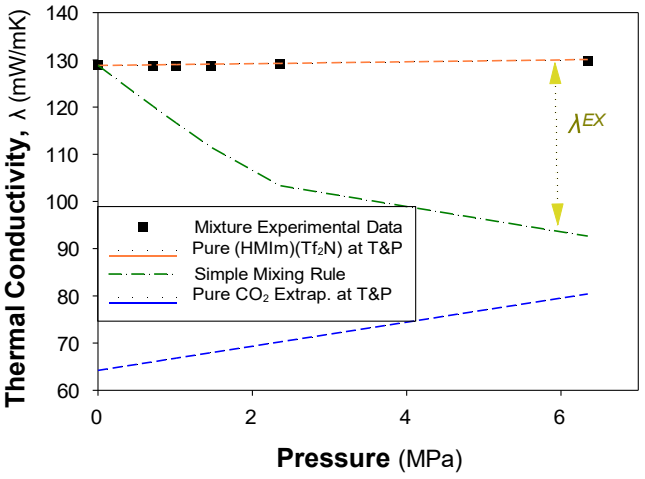

FIGURE 7 Predictions of thermal conductivity at 298.15 K using (1) mixture experimental data, (2) interpolated pure IL data, (3) calculated simple mixing rule, and pure CO_2 extrapolated data. Smoothed lines

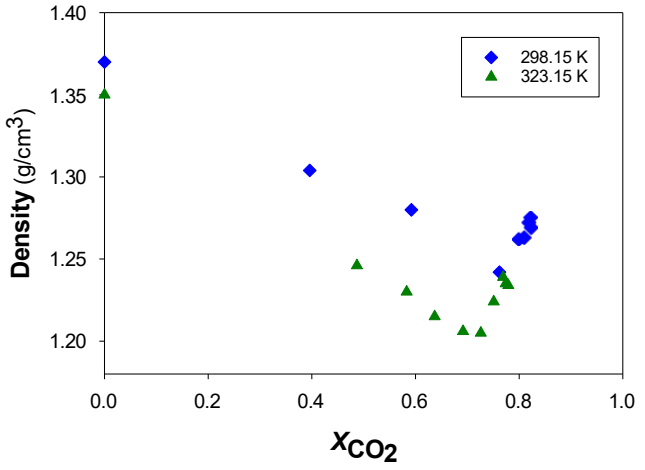

FIGURE 8 Mass density of [HMIm][Tf_2N]/CO_2 at various compositions at ◆) 298.15 K; ▲) 323.15 K. Data from Ren et al.[63] [HMIm][Tf_2N], 1-hexyl-3-methyl-imidazolium bis(trifluoromethylsulfonyl) amide

Both the modified Bridgman and HMET correlations indicate that thermal conductivity is directly proportional to density. Ren and Scurto[113] report the volume expansion, liquid molar volumes, and densities for [HMIm][Tf_2N] saturated with compressed CO_2 at various temperatures and pressures. The IL does experience a moderate volume expansion with increased CO_2 dissolution with increasing pressure. For instance, at ~3.6 MPa, the IL expands its volume by ~17% at 298.15 K and ~11% at 323.15 K; these conditions correspond to a liquid CO_2 composition of ~60%mole at 298.15 K and 49%mole CO_2 at 323.15 K. However, despite the volume expansion, the molar volume decreases relatively linearly at both isotherms with increasing CO_2 composition; that is, molar density increases as more moles of CO_2 dissolve compared to the commensurate volume expansion. However, with the asymmetry in the molecular mass between the IL and CO_2, the mass density actually decreases to a minimum before beginning to increase at the highest CO_2 compositions (pressures) as shown in Figure 8. The minimum at both 298.15 and 323.15 K occurs at approximately 70% CO_2 composition in the liquid phase. Interestingly, the minimum in thermal conductivity of the [HMIm][Tf_2N]/CO_2 system occurs at approximately 40% mole CO_2 at the same isotherms. It should be noted that the Bridgman equation relates thermal conductivity to density, speed of sound, and isochoric heat capacity. The experimental speed of sound and heat capacity for the [HMIm][Tf_2N]/CO_2 system has not been reported in the literature. However, for the system of 1-butyl-3-methylimidazolium bis(trifluoromethylsulfonyl)amide ([BMIm][Tf_2N]) and CO_2, the speed of sound was measured at 313.15 K and decreases by ~18% at 10 MPa (~73% mole CO_2) where it reaches a relative minimum followed by an increase in the speed of sound at higher pressures and compositions.[121] Neither of these reported minima in the speed of sound or density are exactly near the reported minima here for thermal conductivity, but it does illustrate how the Bridgman equation would qualitatively predict a minimum at each isotherm.

4 | CONCLUSIONS

The thermal conductivity of the IL [HMIm][Tf_2N] saturated with CO_2 at three isotherms (298.15, 323.15, 348.15 K) and pressures ranging up to 19.7 MPa was measured. The thermal conductivity decreases slightly with increasing CO_2 compositions in lower composition regimes and increases gradually in the moderate to high composition regimes. The increase in thermal conductivity at moderate and high CO_2 compositions is attributed to hydrostatic pressure effects, in which it is hypothesized that the increase in thermal conductivity of the liquid due to the increase in hydrostatic pressure outweighs the decrease associated with increased CO_2 composition. Nevertheless, the change in thermal conductivity in the biphasic [HMIm][Tf_2N]/CO_2 system remains dominated by that of the pure IL even at higher compositions of dissolved CO_2. This behavior is attributed to the nature of the mechanism in which CO_2 dissolves in the IL; in which, it is believed that the CO_2 dissolves in the IL primarily by occupying the free volume in the IL. Therefore, the CO_2 does not seem to alter the intramolecular interactions of the IL (cation–anion or between other cations–anions). This behavior indicates that simple mixing rules based on the properties of the pure components and their relative compositions in the mixture are not appropriate in predicting the thermal conductivity of the mixture.

ACKNOWLEDGMENTS

We would like to thank the US National Science Foundations (NSF) for financial support under grants: EEC-1852308, EFRI-2029354, and CBET-1917480. We would like to thank Mr. Scott Ramskill for help in mechanical troubleshooting. Dr. Rajkumar Kore is thanked for his aid in the NMR purity studies.

AUTHOR CONTRIBUTIONS

Karim S. Al-Barghouti: Data curation (lead); formal analysis (lead); investigation (lead); methodology (supporting); visualization (lead); writing – original draft (lead); writing – review and editing (supporting). Aaron M. Scurto: Conceptualization (lead); data curation (supporting); formal analysis (equal); investigation (supporting); methodology (lead); project administration (lead); resources (lead); supervision (lead); writing – original draft (supporting); writing – review and editing (lead).

DATA AVAILABILITY STATEMENT

The data that support the findings of this study are available from the corresponding author upon reasonable request.

ORCID

Karim S. Al-Barghouti https://orcid.org/0000-0002-6167-1516
Aaron M. Scurto https://orcid.org/0000-0001-7214-1871

REFERENCES

1. Maton C, De Vos N, Stevens CV. Ionic liquid thermal stabilities: decomposition mechanisms and analysis tools. *Chem Soc Rev*. 2013;42(13):5963.
2. Steinrück H-P, Wasserscheid P. Ionic liquids in catalysis. *Catal Lett*. 2015;145(1):380-397.
3. Ahosseini A, Ren W, Scurto AM. Understanding biphasic ionic liquid/CO_2 systems for homogeneous catalysis: hydroformylation. *Ind Eng Chem Res*. 2009;48(9):4254-4265.
4. Li J, Li T, Peng C, Liu H. Extractive distillation with ionic liquid entrainers for the separation of acetonitrile and water. *Ind Eng Chem Res*. 2019;58(14):5602-5612.
5. Watanabe M, Thomas ML, Zhang S, Ueno K, Yasuda T, Dokko K. Application of ionic liquids to energy storage and conversion materials and devices. *Chem Rev*. 2017;117(10):7190-7239.
6. Qi H, Ren Y, Guo S, et al. High-voltage resistant ionic liquids for lithium-ion batteries. *ACS Appl Mater Interfaces*. 2020;12(1):591-600.
7. Talebi M, Patil R, Armstrong DW. Gas chromatography columns using ionic liquids as stationary phase. In: Shiflett M, ed. *Commercial Applications of Ionic Liquids. Green Chemistry and Sustainable Technology*. Springer, Cham; 2020.
8. Shiflett MB, Corbin DR, Elliott BA, Yokozeki A. Sorption of trifluoromethane in zeolites and ionic liquid. *J Chem Thermodyn*. 2013;64:40-49.

9. Shiflett MB, Niehaus AMS, Yokozeki A. Separation of N_2O and CO_2 using room-temperature ionic liquid [bmim][BF_4]. *J Phys Chem B*. 2011;115(13):3478-3487.
10. Shiflett MB, Shiflett AD, Yokozeki A. Separation of tetrafluoroethylene and carbon dioxide using ionic liquids. *Sep Purif Tech*. 2011;79(3): 357-364.
11. Shiflett MB, Yokozeki A. Separation of CO_2 and H_2S using room-temperature ionic liquid [bmim][PF_6]. *Fluid Phase Equilib*. 2010; 294(1–2):105-113.
12. Shiflett MB, Yokozeki A. Separation of carbon dioxide and sulfur dioxide using room-temperature ionic liquid [bmim][$MeSO_4$]. *Energy Fuel*. 2010;24(2):1001-1008.
13. Shiflett MB, Yokozeki A. Utilizing ionic liquids for hydrofluorocarbon separation. US patent 8,628,644 B2. 2006.
14. Yokozeki A, Shiflett MB. Separation of carbon dioxide and sulfur dioxide gases using room-temperature ionic liquid [hmim][Tf_2N]. *Energy Fuel*. 2009;23(9):4701-4708.
15. Yokozeki A, Shiflett MB, Junk CP, Grieco LM, Foo T. Physical and chemical absorptions of carbon dioxide in room-temperature ionic liquids. *J Phys Chem B*. 2008;112(51):16654-16663.
16. Afzal W, Liu X, Prausnitz JM. Physical data for a process to separate krypton from air by selective absorption in an ionic liquid. *Fluid Phase Equilib*. 2015;404:124-130.
17. Shiflett MB, Yokozeki A. Absorption cycle utilizing ionic liquid as working fluid. US patent WO2006084262A1. 2006.
18. Boesmann A, Schubert T, Inventors. Absorption Refrigeration Machines and Heat Transformers,. WIPO patent 2005113702A1.
19. Chen F-F, Huang K, Zhou Y, et al. Multi-molar absorption of CO_2 by the activation of carboxylate groups in amino acid ionic liquids. *Angew Chemie Int Ed*. 2016;55(25):7166-7170.
20. Aghaie M, Rezaei N, Zendehboudi S. A systematic review on CO_2 capture with ionic liquids: current status and future prospects. *Renew Sust Energy Rev*. 2018;96:502-525.
21. Bates ED, Mayton RD, Ntai I, Davis JH. CO_2 capture by a task-specific ionic liquid. *J Am Chem Soc*. 2002;124(6):926-927.
22. Ramdin M, De Loos TW, Vlugt TJH. State-of-the-art of CO_2 capture with ionic liquids. *Ind Eng Chem Res*. 2012;51(24):8149-8177.
23. Shannon MS, Bara JE. Properties of Alkylimidazoles as solvents for CO_2 capture and comparisons to imidazolium-based ionic liquids. *Ind Eng Chem Res*. 2011;50(14):8665-8677.
24. Zhou L, Fan J, Shang X. CO2 capture and separation properties in the ionic liquid 1-n-butyl-3-methylimidazolium nonafluorobutylsulfonate. *Materials*. 2014;7(5):3867-3880.
25. Shiflett MB, Drew DW, Cantini RA, Yokozeki A. Carbon dioxide capture using ionic liquid 1-butyl-3-methylimidazolium acetate. *Energy Fuel*. 2010;24(10):5781-5789.
26. Shukla SK, Khokarale SG, Bui TQ, Mikkola J-PT. Ionic liquids: potential materials for carbon dioxide capture and utilization. *Front Mater*. 2019;6:42.
27. Torralba-Calleja E, Skinner J, Gutiérrez-Tauste D. CO_2 capture in ionic liquids: a review of solubilities and experimental method. *J Chem*. 2013;2013:1-16.
28. Brennecke JF, Gurkan BE. Ionic liquids for CO_2 capture and emission reduction. *J Phys Chem Lett*. 2010;1(24):3459-3464.
29. Kanniche M, Gros-Bonnivard R, Jaud P, Valle-Marcos J, Amann J-M, Bouallou C. Pre-combustion, post-combustion and oxy-combustion in thermal power plant for CO_2 capture. *Appl Therm Eng*. 2010;30(1):53-62.
30. Liu X, Huang Y, Zhao Y, Gani R, Zhang X, Zhang S. Ionic liquid design and process simulation for decarbonization of shale gas. *Ind Eng Chem Res*. 2016;55(20):5931-5944.
31. Ren W. *High-Pressure Phase Equilibria of Ionic Liquids and Compressed Gases for Applications in Reactions and Absorption Refrigeration* (PhD Dissertation), University of Kansas. 2009.
32. Martín A, Bermejo MD. Thermodynamic analysis of absorption refrigeration cycles using ionic liquid + supercritical CO_2 pairs. *J Supercrit Fluids*. 2010;55(2):852-859.
33. Sen M, Paolucci S. Using Carbon Dioxide and Ionic Liquids for Absorption Refrigeration. 7th IIR Gustav Lorentzen Conference on Natural Working Fluids. Trondheim, Norway. 2006.
34. Wu W-D, Wu J, Hou Y, Su L, Zhang H. Predicting CO_2 solubility in imidazole ionic liquids for use in absorption refrigeration systems by using the group contribution equation of state method. *Int J Thermophys*. 2017;38:14.
35. NIST Standard Reference Database 23: Reference Fluid Thermodynamic and Transport Properties-REFPROP, Version 10.0, National Institute of Standards and Technology, Standard Reference Data Program, Gaithersburg [computer program]. 2018.
36. Scurto AM, Subramaniam B, Hutchenson K. Gas-Expanded Liquids (GXLs): Fundamentals and Applications in Gas Expanded Liquids and Near-Critical Media: Green Chemistry and Engineering; In: Hutchenson K, Scurto AM, Subramaniam B, eds. *ACS Symposium Series* 1006: Washington, D.C., 2009; Ch. 1, p. 3-37.
37. Sellin MF, Webb PB, Cole-Hamilton DJ. Continuous flow homogeneous catalysis: hydroformylation of alkenes in supercritical fluid–ionic liquid biphasic mixtures. *Chem Commun*. 2001;8: 781-782.
38. Ballivet-Tkatchenko D, Picquet M, Solinas M, Franciò G, Wasserscheid P, Leitner W. Acrylate dimerisation under ionic liquid–supercritical carbon dioxide conditions. *Green Chem*. 2003;5(2):232-235.
39. Bösmann A, Franciò G, Janssen E, Solinas M, Leitner W, Wasserscheid P. Activation, tuning, and immobilization of homogeneous catalysts in an ionic liquid/compressed CO_2 continuous-flow system. *Angew Chemie Int Ed*. 2001;40(14):2697-2699.
40. Brown RA, Pollet P, McKoon E, Eckert CA, Liotta CL, Jessop PG. Asymmetric hydrogenation and catalyst recycling using ionic liquid and supercritical carbon dioxide. *J Am Chem Soc*. 2001;123(6):1254-1255.
41. Jessop PG. Homogeneous catalysis and catalyst recovery using supercritical carbon dioxide and ionic liquids. *J Syn Org Chem Jpn*. 2003;61(5):484-488.
42. Lozano P, De Diego T, Carrie D, Vaultier M, Iborra JL. Lipase catalysis in ionic liquids and supercritical carbon dioxide at 150 °C. *Biotechnol Prog*. 2003;19(2):380-382.
43. Lozano P, Diego TD, Carrié D, Vaultier M, Iborra JL. Continuous green biocatalytic processes using ionic liquids and supercritical carbon dioxide. *Chem Commun*. 2002;7:692-693.
44. Sellin MF, Bach I, Webster JM, et al. Hydroformylation of alkenes in supercritical carbon dioxide catalysed by rhodium trialkylphosphine complexes. *J Chem Soc Dalt Trans*. 2002;24:4569.
45. Solinas M, Pfaltz A, Cozzi PG, Leitner W. Enantioselective hydrogenation of imines in ionic liquid/carbon dioxide media. *J Am Chem Soc*. 2004;126(49):16142-16147.
46. Jutz F, Andanson J-M, Baiker A. Ionic liquids and dense carbon dioxide: a beneficial biphasic system for catalysis. *Chem Rev*. 2011; 111(2):322-353.
47. Zayed F, Greiner L, Schulz PS, Lapkin A, Leitner W. Continuous catalytic Friedel–crafts acylation in the biphasic medium of an ionic liquid and supercritical carbon dioxide. *Chem Commun*. 2008;1:79-81.
48. Ahosseini A, Ren W, Scurto AM. Hydrogenation in biphasic ionic liquid/CO2 systems in Gas Expanded Liquids and Near-Critical Media: Green Chemistry and Engineering. In: Hutchenson K, Scurto AM, Subramaniam B, eds. *ACS Symposium Series* 1006: Washington, D.C., 2009; Chap. 11, p. 218-234.
49. Yokozeki A, Shiflett MB. Gas solubilities in ionic liquids using a generic van der Waals equation of state. *J Supercrit Fluids*. 2010; 55(2):846-851.
50. Anderson JL, Dixon JK, Brennecke JF. Solubility of CO_2, CH_4, C_2H_6, C_2H_4, O_2, and N_2 in 1-hexyl-3-methylpyridinium Bis(trifluoromethylsulfonyl) imide: comparison to other ionic liquids. *Acc Chem Res*. 2007;40(11): 1208-1216.
51. Anthony JL, Anderson JL, Maginn EJ, Brennecke JF. Anion effects on gas solubility in ionic liquids. *J Phys Chem B*. 2005;109(13):6366-6374.

52. Carvalho PJ, Coutinho JAP. The polarity effect upon the methane solubility in ionic liquids: a contribution for the design of ionic liquids for enhanced CO_2/CH_4 and H_2S/CH_4 selectivities. *Energ Environ Sci*. 2011;4(11):4614.
53. Carvalho PJ, Regueira T, Fernández J, et al. High pressure density and solubility for the CO_2+1-ethyl-3-methylimidazolium ethylsulfate system. *J Supercrit Fluids*. 2014;88:46-55.
54. Lemus J, Da Silva FFA, Palomar J, Carvalho PJ, Coutinho JAP. Solubility of carbon dioxide in encapsulated ionic liquids. *Sep Purif Tech*. 2018;196:41-46.
55. Liu X, O'Harra KE, Bara JE, Turner CH. Solubility behavior of CO_2 in ionic liquids based on ionic polarity index analyses. *J Phys Chem B*. 2021;125(14):3665-3676.
56. Llovell F, Oliveira MB, Coutinho JAP, Vega LF. Solubility of greenhouse and acid gases on the $[C_4mim][MeSO_4]$ ionic liquid for gas separation and CO_2 conversion. *Catal Today*. 2015;255:87-96.
57. Mejía I, Stanley K, Canales R, Brennecke JF. On the high-pressure solubilities of carbon dioxide in several ionic liquids. *J Chem Eng Data*. 2013;58(9):2642-2653.
58. Safarov J, Abdullayeva G, Bashirov M, Tuma D, Bashirov R. The ionic liquid 1-ethyl-3-methylimidazolium methanesulfonate revisited: solubility of carbon dioxide over an extended range of temperature and pressure. *J Mol Liq*. 2021;333:115920.
59. Blanchard LA, Gu Z, Brennecke JF. High-pressure phase behavior of ionic liquid/CO_2 systems. *J Phys Chem B*. 2001;105(12):2437-2444.
60. Cadena C, Anthony JL, Shah JK, Morrow TI, Brennecke JF, Maginn EJ. Why is CO_2 so soluble in imidazolium-based ionic liquids? *J Am Chem Soc*. 2004;126(16):5300-5308.
61. Scovazzo P, Camper D, Kieft J, Poshusta J, Koval C, Noble R. Regular solution theory and CO_2 gas solubility in room-temperature ionic liquids. *Ind Eng Chem Res*. 2004;43(21):6855-6860.
62. Costa Gomes MF. Low-pressure solubility and thermodynamics of solvation of carbon dioxide, ethane, and hydrogen in 1-hexyl-3-methylimidazolium bis(trifluoromethylsulfonyl)amide between temperatures of 283 K and 343 K. *J Chem Eng Data*. 2007;52(2):472-475.
63. Ren W, Sensenich B, Scurto AM. High-pressure phase equilibria of {carbon dioxide (CO2)+n-alkyl-imidazolium bis(trifluoromethylsulfonyl) amide} ionic liquids. *J Chem Thermodyn*. 2010;42(3):305-311.
64. Turnaoglu T, Minnick DL, Morais ARC, et al. High-pressure vapor-liquid equilibria of 1-Alkyl-1-Methylpyrrolidinium Bis(trifluoromethylsulfonyl) imide ionic liquids and CO2. *J Chem Eng Data*. 2019;64(11):4668-4678.
65. Ahosseini A, Ortega E, Sensenich B, Scurto AM. Viscosity of n-alkyl-3-methyl-imidazolium bis(trifluoromethylsulfonyl)amide ionic liquids saturated with compressed CO_2. *Fluid Phase Equilib*. 2009;286(1):72-78.
66. Morais ARC, Alaras LM, Baek DL, Fox RV, Shiflett MB, Scurto AM. Viscosity of 1-alkyl-1-methylpyrrolidinium bis(trifluoromethylsulfonyl) imide ionic liquids saturated with compressed CO_2. *J Chem Eng Data*. 2019;64(11):4658-4667.
67. Shiflett MB, Yokozeki A. Solubilities and diffusivities of carbon dioxide in ionic liquids: [bmim][PF_6] and [bmim][BF_4]. *Ind Eng Chem Res*. 2005;44(12):4453-4464.
68. Barghi SH, Tsotsis TT, Sahimi M. Solubility and diffusivity of H_2 and CO_2 in the ionic liquid [bmim][PF_6]. *Int J Hydrogen Energy*. 2015;40(28):8713-8720.
69. Friedrich MF, Kokolakis S, Lucas M, Claus P. Measuring diffusion and solubility of slightly soluble gases in [CnMIM][NTf_2] ionic liquids. *J Chem Eng Data*. 2016;61(4):1616-1624.
70. Morgan D, Ferguson L, Scovazzo P. Diffusivities of gases in room-temperature ionic liquids: data and correlations obtained using a lag-time technique. *Ind Eng Chem Res*. 2005;44(13):4815-4823.
71. Moya C, Palomar J, Gonzalez-Miquel M, Bedia J, Rodriguez F. Diffusion coefficients of CO_2 in ionic liquids estimated by gravimetry. *Ind Eng Chem Res*. 2014;53(35):13782-13789.
72. Shokouhi M, Adibi M, Jalili AH, Hosseini-Jenab M, Mehdizadeh A. Solubility and diffusion of H_2S and CO_2 in the ionic liquid 1-(2-hydroxyethyl)-3-methylimidazolium Tetrafluoroborate. *J Chem Eng Data*. 2010;55(4):1663-1668.
73. Zubeir LF, Romanos GE, Weggemans WMA, Iliev B, Schubert TJS, Kroon MC. Solubility and diffusivity of CO_2 in the ionic liquid 1-Butyl-3-methylimidazolium tricyanomethanide within a large pressure range (0.01 MPa to 10 MPa). *J Chem Eng Data*. 2015;60(6):1544-1562.
74. Gonzalez-Miquel M, Bedia J, Palomar J, Rodriguez F. Solubility and diffusivity of CO_2 in [hxmim][NTf_2], [omim][NTf_2], and [dcmim][NTf_2] at T = (298.15, 308.15, and 323.15) K and pressures up to 20 bar. *J Chem Eng Data*. 2014;59(2):212-217.
75. Frez C, Diebold GJ, Tran CD, Yu S. Determination of thermal diffusivities, thermal conductivities, and sound speeds of room-temperature ionic liquids by the transient grating technique. *J Chem Eng Data*. 2006;51(4):1250-1255.
76. Fröba AP, Rausch MH, Krzeminski K, Assenbaum D, Wasserscheid P, Leipertz A. Thermal conductivity of ionic liquids: measurement and prediction. *Int J Thermophys*. 2010;31(11–12):2059-2077.
77. Ge R, Hardacre C, Nancarrow P, Rooney DW. Thermal conductivities of ionic liquids over the temperature range from 293 K to 353 K. *J Chem Eng Data*. 2007;52(5):1819-1823.
78. Liu H, Maginn E, Visser AE, Bridges NJ, Fox EB. Thermal and transport properties of six ionic liquids: an experimental and molecular dynamics study. *Ind Eng Chem Res*. 2012;51(21):7242-7254.
79. Tenney CM, Massel M, Mayes JM, Sen M, Brennecke JF, Maginn EJ. A computational and experimental study of the heat transfer properties of nine different ionic liquids. *J Chem Eng Data*. 2014;59(2):391-399.
80. Yebra F, Troncoso J, Romaní L. Thermal conductivity of ionic liquids under pressure. *Fluid Phase Equilib*. 2020;515:112573.
81. Oster K, Jacquemin J, Hardacre C, Ribeiro APC, Elsinawi A. Further development of the predictive models for physical properties of pure ionic liquids: thermal conductivity and heat capacity. *J Chem Thermodyn*. 2018;118:1-15.
82. Gardas RL, Ge R, Goodrich P, Hardacre C, Hussain A, Rooney DW. Thermophysical properties of amino acid-based ionic liquids. *J Chem Eng Data*. 2010;55(4):1505-1515.
83. Koller TM, Schmid SR, Sachnov SJ, Rausch MH, Wasserscheid P, Fröba AP. Measurement and prediction of the thermal conductivity of tricyanomethanide- and tetracyanoborate-based imidazolium ionic liquids. *Int J Thermophys*. 2014;35(2):195-217.
84. Nieto De Castro CA, Lourenço MJV, Ribeiro APC, et al. Thermal properties of ionic liquids and IoNanofluids of imidazolium and pyrrolidinium liquids. *J Chem Eng Data*. 2010;55(2):653-661.
85. Oster K, Goodrich P, Jacquemin J, Hardacre C, Ribeiro APC, Elsinawi A. A new insight into pure and water-saturated quaternary phosphonium-based carboxylate ionic liquids: density, heat capacity, ionic conductivity, thermogravimetric analysis, thermal conductivity and viscosity. *J Chem Thermodyn*. 2018;121:97-111.
86. Rodil E, Arce A, Arce A, Soto A. Measurements of the density, refractive index, electrical conductivity, thermal conductivity and dynamic viscosity for tributylmethylphosphonium and methylsulfate based ionic liquids. *Thermochim Acta*. 2018;664:81-90.
87. Valkenburg MEV, Vaughn RL, Williams M, Wilkes JS. Thermochemistry of ionic liquid heat-transfer fluids. *Thermochim Acta*. 2005;425(1–2):181-188.
88. Zaripov ZI, Gumerov FM, Khairutdinov VF, et al. Thermal conductivity and thermal diffusivity of pyrrolidinium-based ionic liquids at atmospheric pressure. *Fluid Phase Equilib*. 2019;485:135-145.
89. Hezave AZ, Raeissi S, Lashkarbolooki M. Estimation of thermal conductivity of ionic liquids using a perceptron neural network. *Ind Eng Chem Res*. 2012;51(29):9886-9893.

90. Gardas RL, Coutinho JAP. Group contribution methods for the prediction of thermophysical and transport properties of ionic liquids. *AIChE J*. 2009;55(5):1274-1290.
91. Wu K-J, Zhao C-X, He C-H. Development of a group contribution method for determination of thermal conductivity of ionic liquids. *Fluid Phase Equilib*. 2012;339:10-14.
92. Chen Q-L, Wu K-J, He C-H. Thermal conductivities of [EMIM][$EtSO_4$], [EMIM][$EtSO_4$] + C_2H_5OH, [EMIM][$EtSO_4$] + H_2O, and [EMIM][$EtSO_4$] + C_2H_5OH + H_2O at T = (283.15 to 343.15) K. *J Chem Eng Data*. 2013;58(7):2058-2064.
93. Tomida D, Kenmochi S, Tsukada T, Qiao K, Yokoyama C. Thermal conductivities of [bmim][PF_6], [hmim][PF_6], and [omim][PF_6] from 294 to 335 K at pressures up to 20 MPa. *Int J Thermophys*. 2007;28(4):1147-1160.
94. Kian K, Scurto AM. Heat transport properties of CO2-expanded liquids:n-hexane, n-decane, and n-tetradecane. *Ind Eng Chem Res*. 2017;56(44):12822-12832.
95. Tomida D, Kenmochi S, Tsukada T, Qiao K, Yokoyama C. Thermal conductivities of imidazolium-based ionic liquid + CO_2 mixtures. *Int J Thermophys*. 2010;31(10):1888-1895.
96. Rausch MH, Heller A, Herbst J, et al. Mutual and thermal diffusivity of binary mixtures of the ionic liquids [BMIM][$C(CN)_3$] and [BMIM][$B(CN)_4$] with dissolved CO_2 by dynamic light scattering. *J Phys Chem B*. 2014;118(17):4636-4646.
97. Klein T, Piszko M, Lang M, et al. Diffusivities in binary mixtures of [AMIM][NTf_2] ionic liquids with the dissolved gases H_2, He, N_2, CO, CO_2, or Kr close to infinite dilution. *J Chem Eng Data*. 2020;65(8):4116-4129.
98. Roder HM. A transient hot wire thermal conductivity apparatus for fluids. *J Res Natl Inst Stand Technol*. 1981;86:457.
99. Cohen E, Glicksman L. Analysis of the transient hot-wire method to measure thermal conductivity of silica aerogel: influence of wire length, and radiation properties. *J Heat Transfer*. 2014;136(4):041301.
100. Kian K. *Phase Behavior and Transport Properties of Compressed CO_2-Saturated Alkanes: CO_2/n-Hexane, CO_2/n-Decane, and CO_2/n-Tetradecane*. MS Thesis. University of Kansas; 2017.
101. Nwosu S *Environmentally Benign Production of Ionic Liquids in CO_2-Expanded Systems*. PhD Dissertation. University of Kansas; 2012.
102. Carslaw HS, Jaeger JC. *Conduction of Heat in Solids*. 2nd ed. Clarendon; 1959.
103. Qun-Fang L, Rui-Sen L, Dan-Yan N, Yu-Chun H. Thermal conductivities of some organic solvents and their binary mixtures. *J Chem Eng Data*. 1997;42(5):971-974.
104. Assael MJ, Bogdanou I, Mylona SK. Reference correlation of the thermal conductivity of n-heptane from the triple point to 600 K and up to 250 MPa. *J Phys Chem Ref Data Monogr*. 2013;42(2):023101.
105. Paredes X, Queiros C, Santos FJV, et al. Thermophysical properties of 1-hexyl-3-methylimidazolium bis(trifluoromethylsulfonyl)imide, $C_{(6)}$mim $(CF_3SO_2)_{(2)}$N -new data, reference data, and reference correlations. *J Phys Chem Ref Data Monogr*. 2020;49(4):51.
106. Ribeiro APC, SIC V, Goodrich P, Hardacre C, Lourenço MJV, de Castro CAN. Thermal conductivity of [Cn mim][$(CF_3SO_2)_2$N] and [C_4mim][BF_4] IoNanofluids with carbon nanotubes—measurement, theory and structural characterization. *J Nanofluids*. 2013;2:55-62.
107. Wu K-J, Chen Q-L, He C-H. Speed of sound of ionic liquids: database, estimation, and its application for thermal conductivity prediction. *AIChE J*. 2014;60(3):1120-1131.
108. Esperança J, Guedes HJR, Lopes JNC, Rebelo LPN. Pressure-density-temperature(p-rho-T) surface of $C_{(6)}$mim NTf_2. *J Chem Eng Data*. 2008;53(3):867-870.
109. Safarov J, Hamidova R, Zepik S, et al. Thermophysical properties of 1-hexyl-3-methylimidazolium bis(trifluoromethylsulfonyl)imide at high temperatures and pressures. *J Mol Liq*. 2013;187:137-156.
110. Andresová A, Bendová M, Schwarz J, Wagner Z, Feder-Kubis J. Influence of the alkyl side chain length on the thermophysical properties of chiral ionic liquids with a (1 R,2 S,5 R)-(-)-menthol substituent and data analysis by means of mathematical gnostics. *J Mol Liq*. 2017;242:336-348.
111. Polikhronidi NG, Batyrova RG, Abdulagatov IM, Magee JW, Wu J. Thermodynamic properties at saturation derived from experimental two-phase isochoric heat capacity of 1-Hexyl-3-methylimidazolium bis[(trifluoromethyl)sulfonyl]imide. *Int J Thermophys*. 2016;37(11).
112. Huber ML, Sykioti EA, Assael MJ, Perkins RA. Reference correlation of the thermal conductivity of carbon dioxide from the triple point to 1100 K and up to 200 MPa. *J Phys Chem Ref Data Monogr*. 2016;45(1):013102.
113. Ren W, Scurto AM. Global phase behavior of imidazolium ionic liquids and compressed 1,1,1,2-tetrafluoroethane (R-134a). *AIChE J*. 2009;55(2):486-493.
114. Al-Barghouti KS & Scurto AM. Thermal conductivity of imidazolium ionic liquids and compressed 1,1,1,2-tetrafluoroethane. *J Chem Eng Data*. 2022.
115. Muldoon MJ, Aki SNVK, Anderson JL, Dixon JK, Brennecke JF. Improving carbon dioxide solubility in ionic liquids. *J Phys Chem B*. 2007;111(30):9001-9009.
116. Almantariotis D, Gefflaut T, PáDua AAH, Coxam JY, Costa Gomes MF. Effect of fluorination and size of the alkyl side-chain on the solubility of carbon dioxide in 1-alkyl-3-methylimidazolium bis(trifluoromethylsulfonyl)amide ionic liquids. *J Phys Chem B*. 2010;114(10):3608-3617.
117. Gutkowski KI, Shariati A, Peters CJ. High-pressure phase behavior of the binary ionic liquid system 1-octyl-3-methylimidazolium tetrafluoroborate +carbon dioxide. *J Supercri. Fluid.* 2006;39(2):187-191.
118. Liu X, O'Harra KE, Bara JE, Turner CH. Molecular insight into the anion effect and free volume effect of CO_2 solubility in multivalent ionic liquids. *Phys Chem Chem Phys*. 2020;22(36):20618-20633.
119. Llovell F, Vega LF. Assessing ionic liquids experimental data using molecular modeling: [Cnmim][BF_4] case study. *J Chem Eng Data*. 2014;59(10):3220-3231.
120. Shannon MS, Tedstone JM, Danielsen SPO, Hindman MS, Irvin AC, Bara JE. Free volume as the basis of gas solubility and selectivity in imidazolium-based ionic liquids. *Ind Eng Chem Res*. 2012;51(15):5565-5576.
121. Demizu M, Harada M, Saijo K, Terazima M, Kimura Y. Transport properties and solvation structure of mixtures of carbon dioxide and room-temperature ionic liquids. *Bull Chem Soc Jpn*. 2011;84(1):70-78.

How to cite this article: Al-Barghouti KS, Scurto AM. Thermal conductivity of the ionic liquid [HMIm][Tf_2N] with compressed carbon dioxide. *AIChE J*. 2022;e17635. doi:10.1002/aic.17635